

Article

Effect of Sintering Temperature and Applied Load on Anode-Supported Electrodes for SOFC Application

Xuan-Vien Nguyen ^{1,*}, Chang-Tsair Chang ², Guo-Bin Jung ¹, Shih-Hung Chan ¹,
Wilson Chao-Wei Huang ¹, Kai-Jung Hsiao ¹, Win-Tai Lee ³, Shu-Wei Chang ³ and I-Cheng Kao ³

¹ Department of Mechanical Engineering & Fuel Cell Center, Yuan Ze University, Taoyuan 320, Taiwan; guobin@saturn.yzu.edu.tw (G.-B.J.); janshun@saturn.yzu.edu.tw (S.-H.C.); chaowei Huang@gmail.com (W.C.-W.H.); kevin19910927@gmail.com (K.-J.H.)

² Taoyuan Aerotropolis Company, Taoyuan 320, Taiwan; ctchang2858@mail.com

³ Taiwan Power Company, New Taipei City 100, Taiwan; u629790@taipower.com.tw (W.-T.L.); u621250@taipower.com.tw (S.-W.C.); icheng423@gmail.com (I.-C.K.)

* Correspondence: wienheating@gmail.com or s1038705@mail.yzu.edu.tw; Tel.: +886-975-470-278

Academic Editor: Masoud Rokni

Received: 8 June 2016; Accepted: 11 August 2016; Published: 31 August 2016

Abstract: Anode-supported cells are prepared by a sequence of hot pressing and co-sintering processes for solid oxide fuel cell (SOFC) applications. Commercially available porous anode tape (NiO/YSZ = 50 wt %/50 wt %), anode tape (NiO/YSZ = 30 wt %/70 wt %), and YSZ are used as the anode substrate, anode functional layer, and electrolyte layer, respectively. After hot pressing, the stacked layers are then sintered at different temperatures (1250 °C, 1350 °C, 1400 °C and 1450 °C) for 5 h in air. Different compressive loads are applied during the sintering process. An (La,Sr)MnO₃ (LSM) paste is coated on the post-sintered anode-supported electrolyte surface as the cathode, and sintered at different temperatures (1100 °C, 1150 °C, 1200 °C and 1250 °C) for 2 h in air to generate anode-supported cells with dimensions of 60 × 60 mm² (active reaction area of 50 × 50 mm²). SEM is used to investigate the anode structure of the anode-supported cells. In addition, confocal laser scanning microscopy is used to investigate the roughness of the cathode surfaces. At sintering temperatures of 1400 °C and 1450 °C, there is significant grain growth in the anode. Furthermore, the surface of the cathode is smoother at a firing temperature of 1200 °C. It is also found that the optimal compressive load of 1742 Pa led to a flatness of 168 μm/6 cm and a deformation of 0.72%. The open circuit voltage and power density of the anode-supported cell at 750 °C were 1.0 V and 178 mW·cm⁻², respectively.

Keywords: pretreatment; anode-supported cell; solid oxide fuel cell (SOFC); impedance spectra; warpage; applied load; roughness; cell shape

1. Introduction

In recent years, anode-supported planar solid oxide fuel cells (SOFC) have received much attention, owing to their good power density at intermediate temperatures. The main advantages of power production through these SOFCs are the high conversion efficiency, the absence of combustion, and the fuel flexibility that allows for the use of a variety of fuels (including those derived from renewable sources). An SOFC is normally operated at a high temperature range (600–1000 °C). A multilayer tape casting and co-sintering process has been studied to fabricate large-area anode-supported planar single cells consisting of: (a) an anode substrate (Ni-YSZ), to provide good electrical conductivity and sufficient mechanical strength; (b) an anode functional layer, to improve the electrochemical performance; and (c) an ScSZ electrolyte used in the form of a thin film, to reduce the ohmic resistance at lower temperatures [1]. The traditional electrolytes of SOFCs

exhibit sufficient ionic conductivities above 800 °C [2]. Conventional SOFCs with an yttria-stabilized zirconia (YSZ) electrolyte are now being operated at 900 °C or higher temperatures to attain a power density sufficient for use in the system. However, the high-temperature operation causes serious problems, such as internal mechanical stress, due to the difference in the thermal expansion coefficients of the materials, as well as chemical reactions. Therefore, an operating temperature lower than 700 °C is desirable [3]. Nevertheless, because electrochemical and conduction processes in SOFCs are strongly thermally activated, a reduced operating temperature leads to the problem of large voltage losses, due to the ohmic resistance of the materials and polarization at the electrodes. As most of the voltage losses arise from the ohmic resistance of the electrolyte, a number of approaches have been reported for preparing a thinner electrolyte, reducing the corresponding resistance [4,5] and obtaining a high power density when using YSZ thin-film electrolytes [6,7].

Generally, there are two categories of techniques for making a robust anode–electrolyte–cathode cell while maintaining a thin electrolyte layer: a cathode-supported cell [8,9] and an anode-supported cell [10–12]. However, the high operating temperature is restrictive, calling for expensive materials, long start-up and shut-down times, and high running costs, as well as causing thermal stress. These restrictions have hindered the commercialization of SOFCs [13]. Therefore, lowering the operating temperature of SOFCs has attracted increasing interest in recent years [14]. However, the increased electrolyte resistivity at lower temperatures then becomes the major impediment decreasing the performance of the SOFCs [15]. Anode-supported SOFCs are currently widely studied, with Ni/YSZ cermet being the most popular anode material. Ni/YSZ cermet is thermally suitable with the YSZ electrolyte, even if the processing temperature exceeds 1400 °C, allowing for a flexible manufacturing process [16]. Using molecular dynamics in conjunction with an established set of Born model potentials, oxygen diffusion in $\text{Sr}_{0.75}\text{Y}_{0.25}\text{CoO}_{2.625}$ was investigated, an activation energy of diffusion for 1.56 eV was predicted in the temperature range from 1000 K to 1400 K [17]. Energetics in the double perovskite $\text{PrBaCo}_2\text{O}_{5.5}$ were investigated in the temperature range from 650 °C to 1000 °C. An anisotropic oxygen diffusion mechanism with diffusion occurring predominantly in the Pr-O and Co-O layers was observed. An activation energy of $E_a = 0.35$ eV was measured for the range of temperatures under study [18]. Conventional SOFC fabrication involves multiple sintering steps; the manufacturing costs of SOFCs could thus be reduced by employing a single-step co-firing technique. A promising technique is the simultaneous fabrication of the electrolyte and supporting anode [19], followed by co-firing together. This could increase the productivity and decrease the fabrication cost. The expensive and complex processing steps for anode-supported electrolyte tapes could be replaced by cheaper, simpler, and continuous techniques. During the co-sintering process, differences in the thermo-elastic materials properties of YSZ and NiO-YSZ cermets that are bonded together will cause the warpage of the anode-supported cell [20,21]. The flatness of the planar unit cell is crucial to the performance of the planar SOFCs, because a flatter cell offers greater contact area between membrane electrode assembly (MEA) surface and the current-collectors [22,23]. Warpage may affect the successful stack operation, which relies on durable contact between the cell electrodes and the interconnect material [24]. Fabricating flat anode-supported cells are very important for successful SOFC stack assembly and commercialization of planar SOFC technology [25,26]. Many studies have focused on investigating and controlling the warpage; experimental methods have been widely conducted to study the phenomenon [27–29]. Single cells with an anode-supported electrolyte are currently fabricated using the tape-casting/lamination/co-firing (TLC) technique. It should be noted, however, that controlling the flatness of large-sized unit cells prepared by the TLC technique is known to be a challenge because of mismatches between the thermo-mechanical and physical properties of the individual layers [30]. The flatness of a cell is considerably dependent on warp phenomena, which can easily occur during the burn-out and sintering processes. Therefore, the interrelationships between the flatness, warping, and cell performance of anode-supported unit cells prepared by the TLC technique require thorough investigations to improve the performance and durability of SOFCs. Using an applied pressure of 1107.4 Pa during the TLC technique improves the flatness to 55 $\mu\text{m}/5$ cm [22].

To fabricate planar SOFC unit cells cost-effectively, this study has focused on the following topics: (i) an enhancement in the flatness of anode-supported electrolytes via control of the pressure load during anode-supported electrolyte fabrication; (ii) an evaluation of the effects of flatness and deformation on the anode-supported electrolyte; (iii) an evaluation of the effect of firing temperature on the anode-supported electrolyte via control of the compression and co-firing steps during anode-supported electrolyte fabrication; and (iv) an evaluation of the effect of firing temperature on the cathode surface via control of the co-firing steps. In this study, the anode-supported cells were homemade designed and fabricated. The anode-supported electrolyte tapes were sintered at 1250 °C, 1350 °C, 1400 °C and 1450 °C for 5 h in air, and coated tapes were fired at different temperatures (1100 °C, 1150 °C, 1200 °C and 1250 °C) for 2 h in air. An optimal co-sintering temperature of 1400–1450 °C for the anode-supported electrolyte and a sintering temperature of 1200–1250 °C for the (La,Sr)MnO₃-cathode paste are recommended for commercially available anode-electrolyte multilayers for anode-supported SOFCs, in order to achieve acceptable performance. In addition, the effect of applied pressure loads on the warpage behavior of cells has been investigated. The purpose of the present work is to provide a better insight into the flatness behavior of the planar anode-supported cell in the scaling up process.

2. Material and Methods

2.1. Cell Fabrication

Commercial anode material (42421, NiO/YSZ = 50 wt %/50 wt %, thickness 180 µm; ESL Electro-Science Co. Ltd., King of Prussia, PA, USA), anode functional layer material (42420, NiO/YSZ = 30 wt %/70 wt %, thickness 20 µm; ESL Electro-Science Co. Ltd., King of Prussia, PA, USA), and electrolyte material (42400, 8 mol% YSZ, thickness 18 µm; ESL Electro-Science Co. Ltd., King of Prussia, PA, USA) were used to fabricate the anode-supported electrolyte. A flowchart detailing the manufacturing process for fabricating a single SOFC cell, starting from anode-supported electrolyte preparation, is shown schematically in Figure 1a. A single SOFC cell was constructed on a sintered bi-layer by brush painting a porous layer of cathode paste (LSM: La_{0.65}Sr_{0.3}MnO₃) on the YSZ layer, followed by firing at different temperatures (1100 °C, 1150 °C, 1200 °C and 1250 °C) for 2 h. The tri-layer thus formed constitutes a single SOFC cell. The structure of the anode-supported cell is shown in Figure 1b.

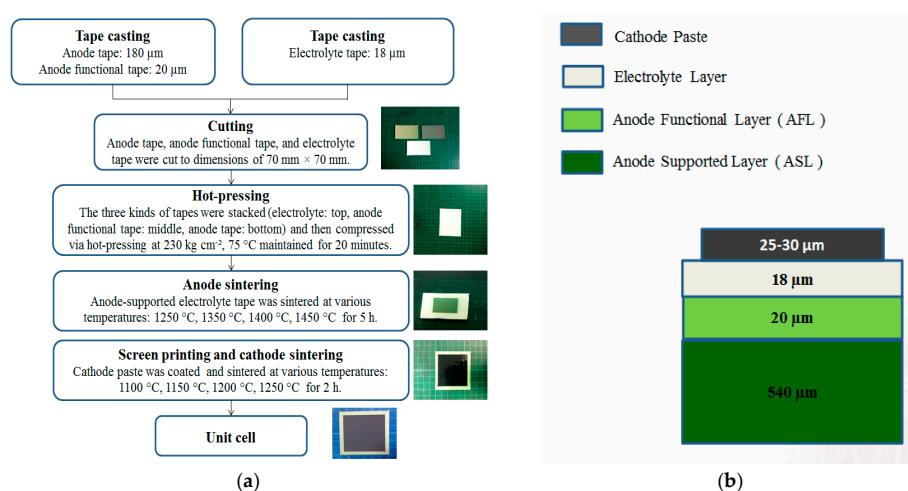


Figure 1. (a) Flowchart of the manufacturing process for the SOFC cell; and (b) structure of the anode-supported cell SOFC.

The anode-supported cell consists of an anode-supported layer with a thickness of 540 µm, an anode functional layer with a thickness of 20 µm, an electrolyte layer with a thickness of

18 μm , and a cathode paste layer with a thickness ranging from 20 μm to 30 μm . The anode layer, anode functional layer, and electrolyte layer were cut to dimensions of 70 mm \times 70 mm. The three kinds of tapes were stacked (electrolyte: top, anode functional layer: middle, anode layer: bottom) and then compressed via hot-pressing at 230 $\text{kg}\cdot\text{cm}^{-2}$, 75 $^{\circ}\text{C}$ maintained for 20 min. The anode-supported electrolyte sample was then allowed to cool at room temperature and weighed to determine the deposit yield. The dried sample was then co-sintered at 1250 $^{\circ}\text{C}$, 1350 $^{\circ}\text{C}$, 1400 $^{\circ}\text{C}$ and 1450 $^{\circ}\text{C}$ for 5 h.

2.1.1. Heat-Treatment of the Anode-Supported Electrolyte

After hot-pressing, the compressed tape was placed in an anode-heating box. The firing profiles are as follows: first, a firing step from 25 $^{\circ}\text{C}$ (room temperature) to 650 $^{\circ}\text{C}$ for 15 h and 30 min with the heating rate controlled at ~ 0.67 $^{\circ}\text{C}\cdot\text{min}^{-1}$; second, a firing step from 650 $^{\circ}\text{C}$ to the target temperature of 1000 $^{\circ}\text{C}$ for 4 h with the heating rate controlled at ~ 1.46 $^{\circ}\text{C}\cdot\text{min}^{-1}$; third, a firing step from 1000 $^{\circ}\text{C}$ to the target temperature of 1400 $^{\circ}\text{C}$ for 5 h with the heating rate controlled at ~ 1.33 $^{\circ}\text{C}\cdot\text{min}^{-1}$; fourth, a firing step to maintain the target temperature of 1400 $^{\circ}\text{C}$ for another 1 h and 50 min; fifth, the firing was decreased from 1400 $^{\circ}\text{C}$ to the target temperature of 700 $^{\circ}\text{C}$ for 4 h; and, finally, cooling [31,32]. The anode-supported firing steps are shown in Figure 2a. A photograph of the final 60 mm \times 60 mm unit of the 540- μm -thick anode-supported electrolyte is shown in Figure 3a.

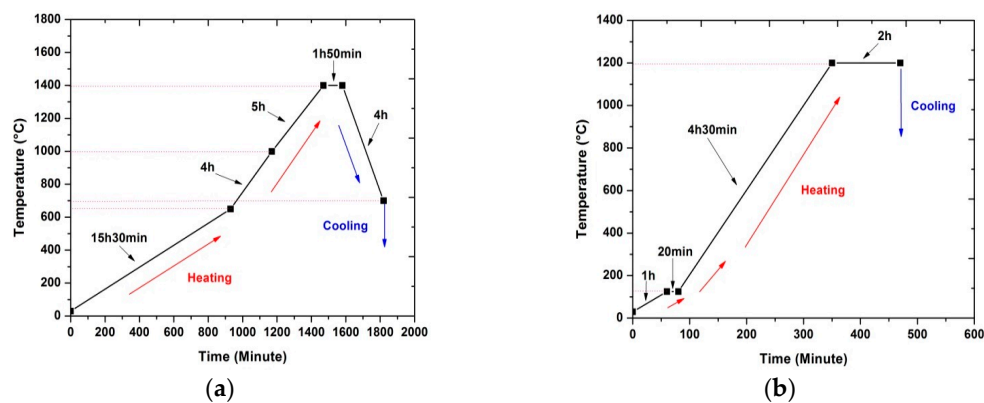


Figure 2. Diagram of the firing profiles for heat treatment of (a) the anode-supported electrolyte and (b) the printed cathode layer.

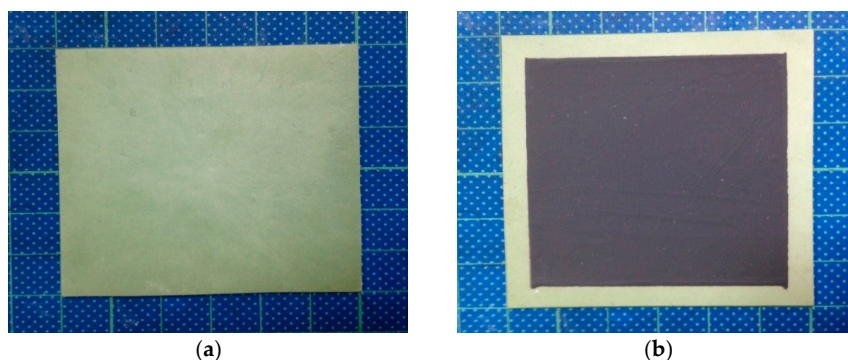


Figure 3. Photograph of the cell unit: (a) the anode-supported electrolyte substrate (after sintering) and (b) the SOFC cell unit (after sintering).

2.1.2. Heat-Treatment of the Cathode

Following the heat treatment, $(\text{La,Sr})\text{MnO}_3$ (LSM) paste (4420, ESL Electro-Science Co. Ltd., King of Prussia, PA, USA), which was selected as the cathode material, was printed onto the YSZ

electrolyte pellets with dimensions of 50 mm × 50 mm. These were then fired in a cathode-heating box. The firing profiles in the cathode-heating box are as follows: first, a firing step from 25 °C (room temperature) to 125 °C for 1 h with the heating rate controlled at ~1.66 °C·min⁻¹; second, a firing step to maintain the target temperature of 125 °C for another 20 min; third, a firing step from 125 °C to the target temperature of 1200 °C for 4 h and 30 min with the heating rate controlled at ~3.98 °C·min⁻¹; fourth, a firing step to maintain the target temperature of 1200 °C for another 2 h; and, finally, cooling [31,32]. The firing steps for the printed cathode are shown in Figure 2b. A photograph of the final 60 mm × 60 mm unit cell is shown in Figure 3b.

2.2. Evaluating the Effects of Flatness and Deformation on the Cell

The flatness (curvature) of the anode-electrolyte tape was evaluated at seven positions in the longitudinal and lateral directions (as shown in Figure 4a). The flatness (curvature) can be calculated by using Equation (1). Figure 4b further illustrates a method to determine the deformation of the anode-electrolyte tape. By using the ratio of the weight of the paper and the anode-supported electrolyte tape (after firing), the rate of the deformation effect for the cell can be found using the following Equation (2):

$$\text{Curvature (flatness)} = b - a \quad (1)$$

where b is the height from the flat surface to the top of anode-supported electrolyte substrate, and a is the thickness of anode-supported electrolyte substrate:

$$\varnothing = \frac{X + Y + Z + W}{\text{Total weight}} \times 100\% \quad (2)$$

where \varnothing is the rate of the deformation effect and X, Y, Z, W are the deformation angles on the four sides of the cell. The deformation angles on the four sides of the cell were determined based on equivalent paper area; and the total weight of the paper is 303 mg.

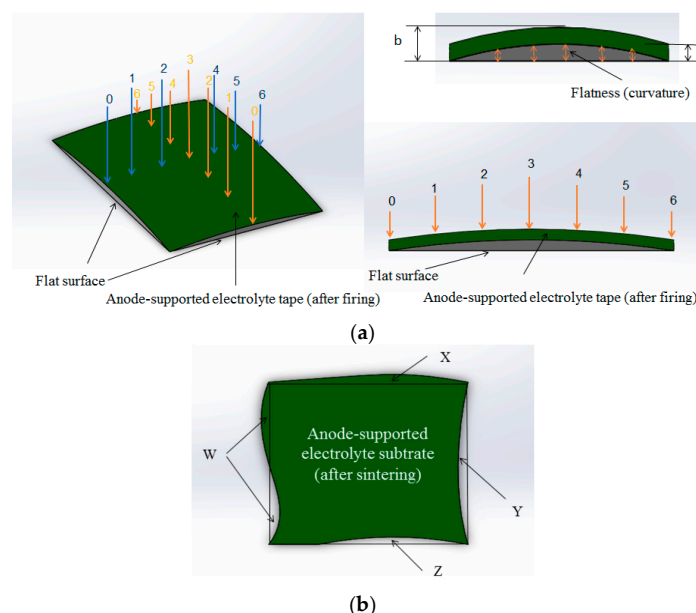


Figure 4. Schematics for the investigation: (a) the flatness of the anode-electrolyte tape; and (b) the deformation of the anode-electrolyte tape.

2.3. Surface Roughness and Microstructural Characterization

The morphology of the anode and cathode surfaces was studied by means of a scanning electron microscope (SEM; JSM-5600, Jeol Co., Akishima, Tokyo, Japan) equipped with an energy-dispersive

spectroscope. The anode surface was coated with gold powder under vacuum. The roughness of the cathode surface was investigated using confocal laser scanning microscopy (CLSM; VK-9710, Keyence Co., Suite 210, Itasca, IL, USA).

2.4. Cell Testing

The test station (TEI-S600-NNNNNS, Tension Energy Inc., Hsin Chu City, Taiwan) was used testing the cell performance. In order to achieve sufficient electrical contact between the cell and the electronic devices, a Ni mesh was used on the anode side and an Ag mesh was used on the cathode side. Two platinum wires were connected to each mesh to serve as the respective voltage and current probes. The cell performance of the anode-supported single cells was tested at 650 °C, 700 °C and 750 °C, according to the following procedure. The temperature was first slowly increased to 750 °C for 15 h anode pretreatment. The system was first fed with mixed gases of nitrogen and 5 vol. % of hydrogen on anode side and air on cathode side as anode pretreatment. The flow rate of nitrogen and hydrogen were 200 mL·min⁻¹, and 20 mL·min⁻¹, respectively. The flow rate of air was 250 mL·min⁻¹. After reaching this temperature, the fuel flow of humidified hydrogen was 300 mL·min⁻¹ (with 3% H₂O) on the anode side, while the flow of air was 500 mL·min⁻¹ on the cathode side. All electrochemical data obtained after the pretreatment were acquired by direct current methods using a current-control power supply and a computer-controlled data acquisition system.

3. Results and Discussion

3.1. Effect of Applied Loads on the Flatness and Deformation of the Anode-Supported Electrolyte

The anode-electrolyte tape was fabricated and fired at 1400 °C, with an anode layer thickness of 540 μm. Various applied loads were placed on the sample to evaluate the dependence of the flatness on the applied load. As shown in Figure 5, when applied loads of 0 g·cm⁻², 14 g·cm⁻², 18 g·cm⁻² and 22 g·cm⁻² were placed, the flatness of the anode-electrolyte tape was 2969 μm/6 cm, 619 μm/6 cm, 168 μm/6 cm and 160 μm/6 cm, respectively. While the 18 g·cm⁻² applied load improved the flatness to 168 μm/6 cm, the 22 g·cm⁻² applied load was better, achieving a flatness of 160 μm/6 cm. However, the 22 g·cm⁻² applied load caused more deformation (as shown in Figure 6d) than the 18 g·cm⁻² applied load. The curvature of the anode-supported electrolyte substrate with applied loads of 0 g·cm⁻², 14 g·cm⁻², 18 g·cm⁻² and 22 g·cm⁻² is shown in Figure 6. The curve of the anode-supported electrolyte substrate with 0 g·cm⁻² is the most pronounced, and the sample warps continuously down with 14 g·cm⁻². The sample quickly flattens at 18 g·cm⁻² and 22 g·cm⁻², and the shape does not change at 18 g·cm⁻². In contrast, the shape of the sample changes with the 22 g·cm⁻² applied load, deforming along each of the four angles.

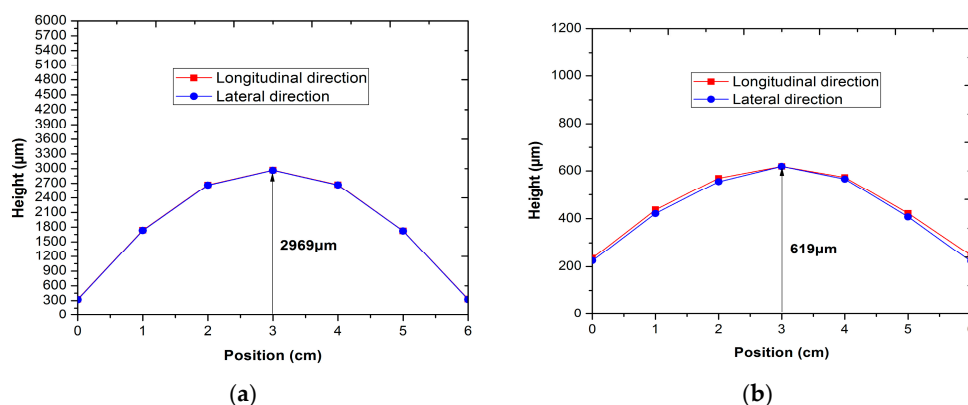


Figure 5. Cont.

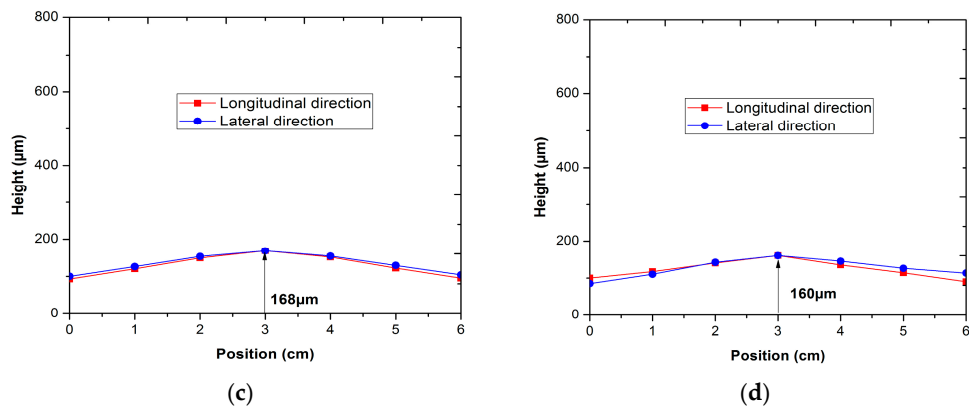


Figure 5. The effect of applied loads on the flatness of the anode-supported electrolyte: (a) $0 \text{ g}\cdot\text{cm}^{-2}$; (b) $14 \text{ g}\cdot\text{cm}^{-2}$; (c) $18 \text{ g}\cdot\text{cm}^{-2}$; and (d) $22 \text{ g}\cdot\text{cm}^{-2}$.

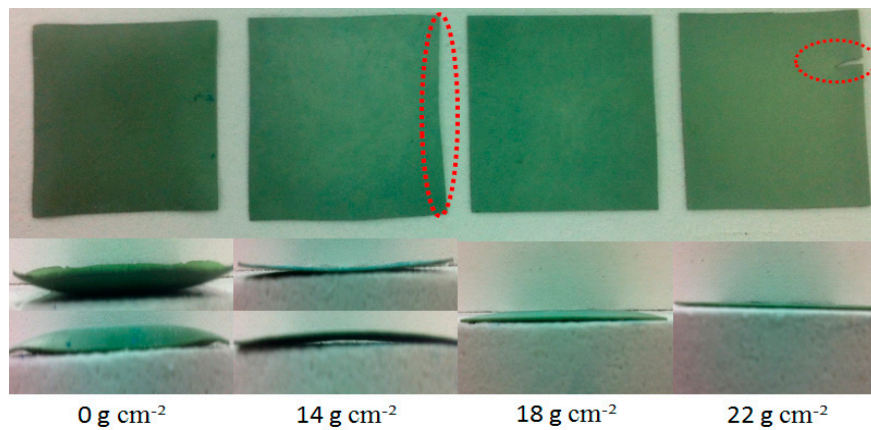


Figure 6. The flatness and deformation of the anode-electrolyte tape with different applied loads.

As shown in Figure 7, the effect of the applied loads on the deformation of the anode-supported electrolyte is calculated by Equation (2). With applied loads of $14 \text{ g}\cdot\text{cm}^{-2}$, $18 \text{ g}\cdot\text{cm}^{-2}$, and $22 \text{ g}\cdot\text{cm}^{-2}$, the deformations of the anode-electrolyte tape are 6.85% ($X = 1.6 \text{ mg}$, $Y = 9.75 \text{ mg}$, $Z = 8.5 \text{ mg}$, $W = 0.9 \text{ mg}$), 0.72% ($X = 1.0 \text{ mg}$, $Y = 0.8 \text{ mg}$, $Z = 0.4 \text{ mg}$), and 3.16% ($X = 2.2 \text{ mg}$, $Y = 2.9 \text{ mg}$, $Z = 3.2 \text{ mg}$, $W = 1.3 \text{ mg}$), respectively.

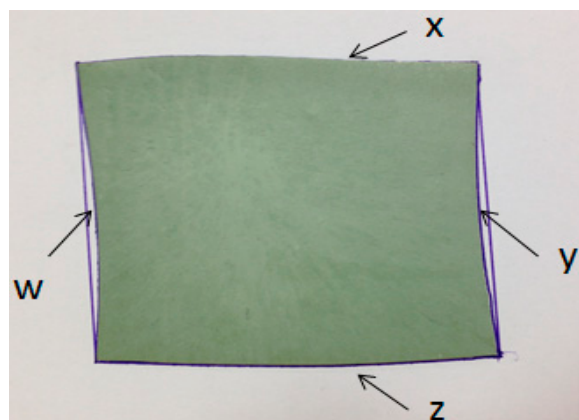


Figure 7. The effect of the applied loads on the deformation of the anode-supported electrolyte substrate.

3.2. Effect of Co-Sintering Temperature on the Microstructural Properties

Figure 8 shows a series of SEM photographs taken at the same magnification ($\times 10,000$), depicting typical areas of the microstructure of each of the samples used in the performance measurements. As observed in Figure 8, the grain size of the anode side sintered at a temperature of $1250\text{ }^{\circ}\text{C}$ is quite small. As the sintering temperature is increased to $1350\text{ }^{\circ}\text{C}$ and $1400\text{ }^{\circ}\text{C}$, there is significant grain growth. The grains do not undergo further growth as the co-sintering temperature is further increased to $1450\text{ }^{\circ}\text{C}$; however, the presence of several small particles indicates significant local agglomeration. The agglomerated particles can be attributed to Ni, which is thermally activated to move freely, especially under a co-sintering temperature higher than $1450\text{ }^{\circ}\text{C}$. The resulting agglomerated Ni leads to insufficient surface area for electrochemical reactions to achieve a high current output. Therefore, the optimal co-firing temperature of anode-electrolyte bilayers is $1400\text{ }^{\circ}\text{C}$. In addition, for the electrode fired at optimal $1400\text{ }^{\circ}\text{C}$, the particle connection of the electrode improved noticeably, while the grain size increased only slightly. Poor connection between electrode particles and/or poor physical contact between the electrolyte and electrode layers may hinder the charge transfer from particle to particle in the electrode, and/or from the electrode to the electrolyte. Figure 9 shows morphological examinations of the cathode interface at temperatures of $1100\text{ }^{\circ}\text{C}$, $1150\text{ }^{\circ}\text{C}$, $1200\text{ }^{\circ}\text{C}$ and $1250\text{ }^{\circ}\text{C}$. As shown in the figure, the grain size at $1200\text{ }^{\circ}\text{C}$ and $1250\text{ }^{\circ}\text{C}$ rapidly increased compared to that at $1100\text{ }^{\circ}\text{C}$ and $1150\text{ }^{\circ}\text{C}$. It was found that the grain size and degree of agglomeration of the powders both increase with the sintering temperature. In particular, the cathode fired at $1200\text{ }^{\circ}\text{C}$, the particle connection of the electrode improved noticeably, while the grain size is suitable in particle connection. If the firing temperature is further increased to $1250\text{ }^{\circ}\text{C}$, the particle agglomerated largely, which will lead to lower surface area and is thus unfavorable for oxygen reduction reaction. Therefore, the optimal firing temperature of cathode bilayers is $1200\text{ }^{\circ}\text{C}$.

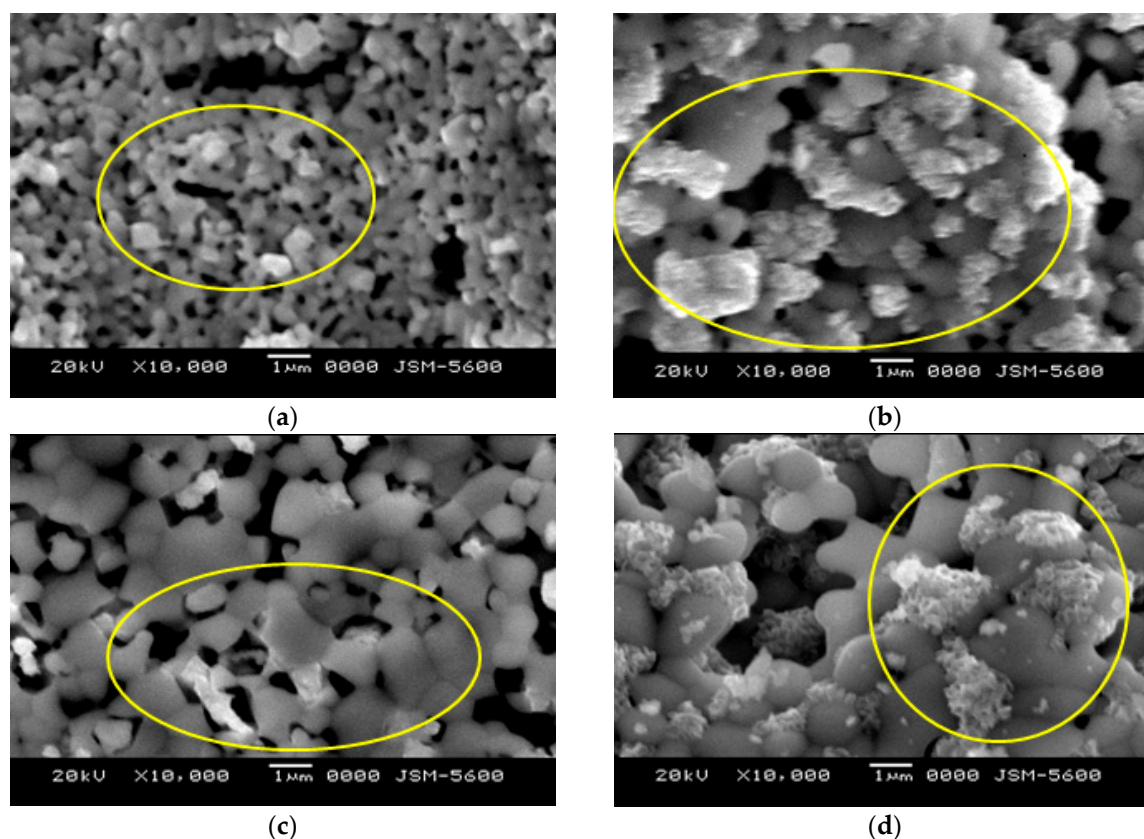


Figure 8. Series of SEM photographs of the anode-electrolyte samples with various sintering temperatures: (a) $1250\text{ }^{\circ}\text{C}$; (b) $1350\text{ }^{\circ}\text{C}$; (c) $1400\text{ }^{\circ}\text{C}$; and (d) $1450\text{ }^{\circ}\text{C}$.

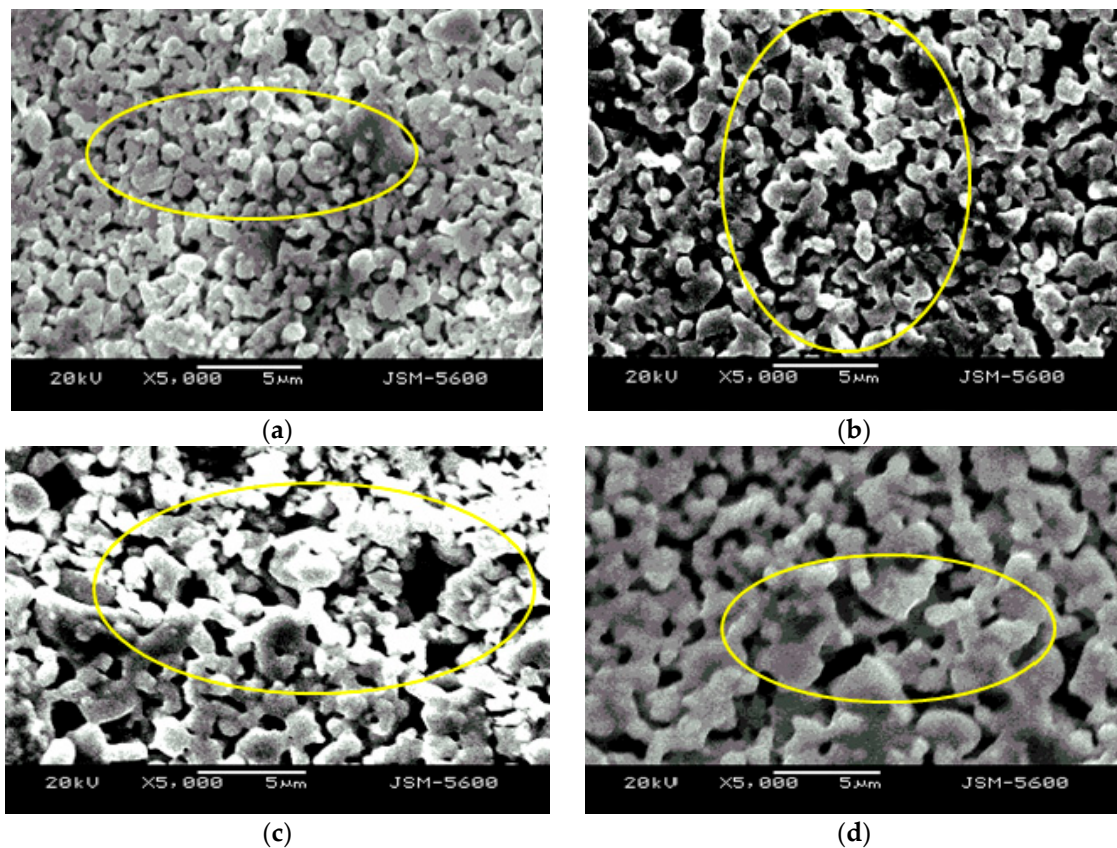


Figure 9. Series of SEM photographs of the cathode interface with various sintering temperatures: (a) 1100 °C; (b) 1150 °C; (c) 1200 °C; and (d) 1250 °C.

3.3. Surface Roughness

Figure 10 shows CLSM images of the cathode surface after firing for the fabrication of SOFC single cells. As shown in Figure 10, the surface of the cathode was quite rough after firing at temperatures of 1100 °C and 1150 °C with a surface roughness of 102.5 µm and 96.5 µm, respectively. As the firing temperature was increased to 1200 °C, the cathode surface became quite smooth, with a surface roughness of 79 µm. However, as the firing temperature was increased to 1250 °C, the cathode had a surface roughness of 82 µm. Moreover, the firing temperature also affected the deformation of the cathode surface.

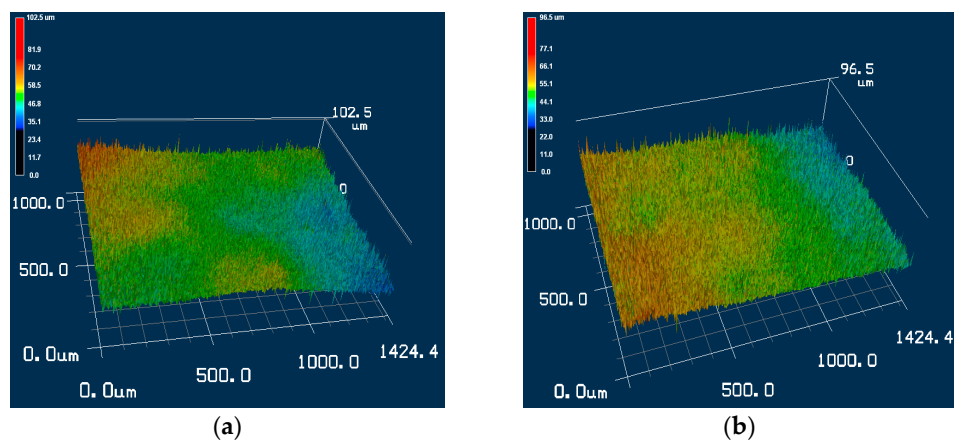


Figure 10. Cont.

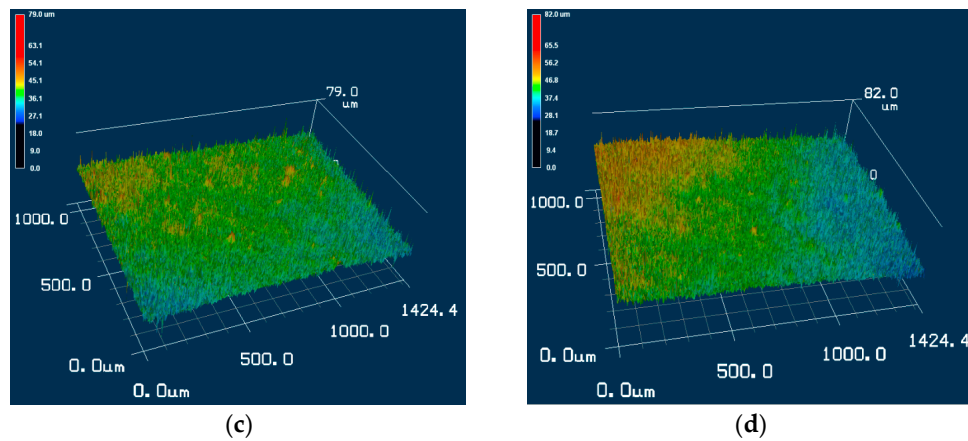


Figure 10. Series of CLSM photographs of the cathode surface with various sintering temperatures: (a) 1100 °C; (b) 1150 °C; (c) 1200 °C; and (d) 1250 °C.

3.4. X-ray Diffraction Pattern

X-ray diffraction (XRD), a non-destructive analytical technique, was used to analyze the crystal structure, chemical composition, and physical properties of the cathode layer. Figure 11 shows the XRD patterns of the cathode-LSM layer after firing at 1100 °C, 1150 °C, 1200 °C and 1250 °C for 2 h. As shown in the figure, the XRD patterns of the cathode-LSM layer after firing at 1100 °C and 1150 °C are quite similar. Likewise, the XRD pattern of the cathode-LSM layer after firing at 1200 °C is quite similar to that at 1250 °C. In addition, diffraction peaks at approximately 28.7°, 47.6°, and 56.4° can be observed. The broad peak at a 2θ value of around 30° indicates the non-crystalline structure or amorphous nature of the composition present in the mixture. The main peaks became sharper at lower temperatures, indicating some grain growth.

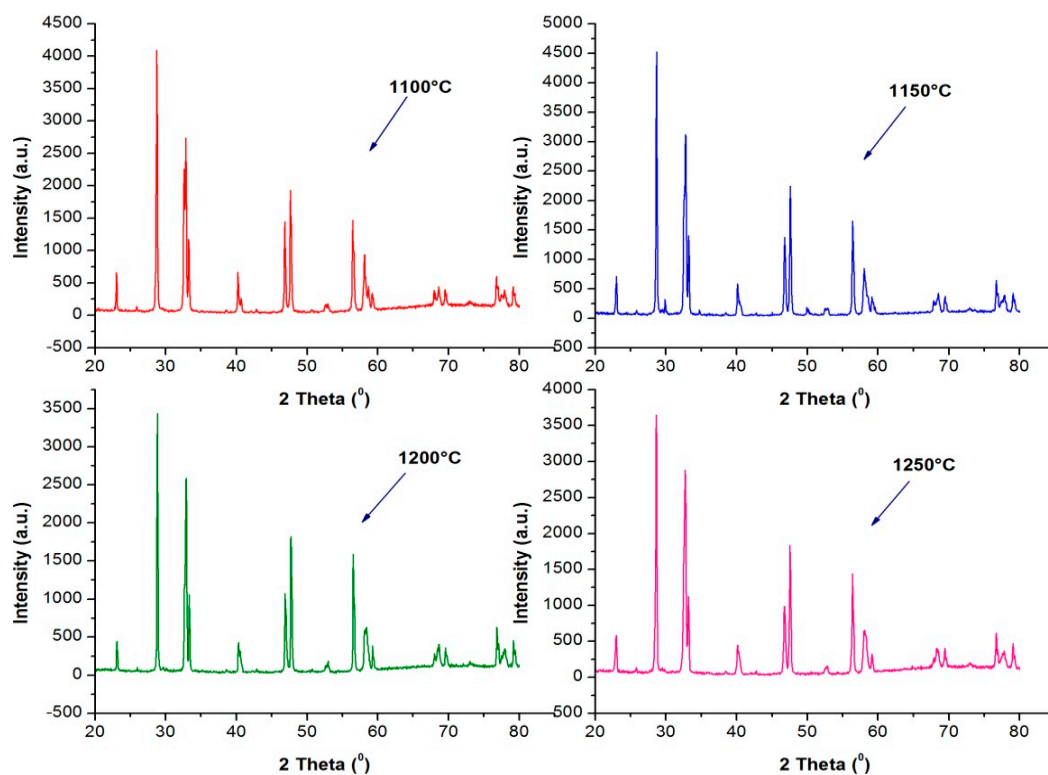


Figure 11. XRD patterns of the LSM cathode, with respect to the firing temperature.

3.5. Cell Performance

Cells were fabricated from anode electrolyte tapes produced with the optimal firing temperature of 1400 °C and a compressive load of 1742 Pa, together with a cathode produced with a firing temperature of 1200 °C. A typical cell with dimensions of 60 × 60 mm² (an active reaction area of 50 × 50 mm²) was used as the standard cell to test the power density. The open circuit voltage (OCV) and power density of the single cell at operating temperatures of 650 °C, 700 °C and 750 °C are shown in Figure 12. The open-circuit voltages (OCV) of the single cell are around 1.0 V, and the maximum power densities of the cell are 105 mW·cm⁻² and 135 mW·cm⁻² at 650 °C and 700 °C, respectively. The maximum power density of the cell are 178 mW·cm⁻² at a voltage of 0.506 V and a total output power of about 4.45 W at 750 °C. It can be seen that the power density of the homemade cell is far below the state-of-the-art in SOFC technology, possibly due to inconsistent cells fabricated manually in the lab. Actually, the cell performance depends on the cell fabrication skill. Currently, we use commercial materials to manually manufacture the cells as such in order to yield consistent cells is a challenge. Nevertheless, the present study shows the effects of sintering temperature and compressive loads on electrodes (flatness, deformation, roughness). Furthermore, the study also shows several methods to investigate and improve electrodes (MEA).

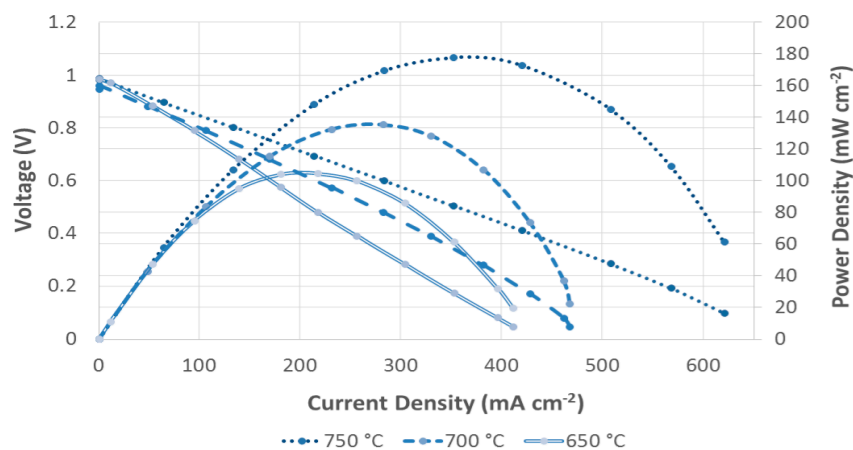


Figure 12. The I - V and I - P curves of the cell.

4. Conclusions

The flatness of a unit cell is critical to the performance of planar SOFCs, as a flatter cell decreases fuel leakage from the anode chamber to the cathode chamber and also increases the contact area of the current collectors. Severely warped specimens cannot be applied to planar SOFC systems. There is thus a need to develop a specific technique for improving the flatness of large unit cells during heat treatment. In this paper, varying applied loads were applied to anode-supported electrolytes to evaluate how the flatness of a sample depends on the pressure. In particular, it was found that an applied load of 18 g·cm⁻² improved the flatness to 168 μm/6 cm.

In addition, the co-sintering temperature was demonstrated to have a pronounced effect on the fabrication and characteristics of an anode-supported electrolyte. At a co-sintering temperature of as low as 1250 °C, the electrolyte was unable to sinter fully, forming a porous structure that led to a reduced open-circuit potential and poor cell performance, along with a low current output. At a co-sintering temperature higher than 1450 °C, the cells were decayed, particularly under high current density operation, due to over-agglomeration of the anode structure. Based on scanning electron microscopy, confocal laser scanning microscopy, and X-ray diffraction data, an optimal co-sintering temperature of 1400–1450 °C for the anode-supported electrolyte and a sintering temperature of 1200–1250 °C for the (La,Sr)MnO₃-cathode paste are recommended for commercially available anode-electrolyte multilayers for anode-supported SOFCs, in order to achieve acceptable

performance. In addition, a single cell made of a 5 cm × 5 cm unit cell in an active area based on the above conditions was tested. The performance of the anode-supported single cell is around 1.0 V. The maximum power density of the cell is 178 mW·cm⁻² at a voltage of 0.506 V, and its total output power at 750 °C is about 4.45 W. The power density of the homemade cell is far below the state-of-the-art in SOFC technology, possibly due to inconsistent cells fabricated manually in the lab. Actually, the cell performance depends on the cell fabrication skill. In addition, the OCV values of the anode-supported SOFC in humidified H₂ less than 1.0 V. They were a little lower than the theoretical values predicted by the Nernst Equation, further indicating that the YSZ membrane was dense, as any leakage in the electrolyte membrane would lead to severely lowering of the OCV values. The lower OCV values may relate to gas leakage at the seals. With this feasibility study, in future work, we believe that it is essential for the SOFC community to use commercially available materials instead of materials developed by individual groups, in order to speed up the research and development of anode-supported SOFC technology.

Acknowledgments: The authors gratefully thank the National Science Council (NSC) of Taiwan under contracts NSC 99-2221-E-155-063 and NSC 100-3113-E-155-001, and the Taiwan Power Company for their financial support.

Author Contributions: Xuan-Vien Nguyen proposed the research, implemented all experiments, wrote and revised the paper. Chang-Tsair Chang, Guo-Bin Jung, Shih-Hung Chan supervised the research. Wilson Chao-Wei Huang, Kai-Jung Hsiao prepared the figures. Win-Tai Lee, Shu-Wei Chang, I-Cheng Kao provided the materials.

Conflicts of Interest: The authors declare no conflict of interest.

Abbreviations

SOFC	Solid oxide fuel cell
SEM	Scanning electron microscopy
CLSM	Confocal laser scanning microscopy
XRD	X-ray diffraction

References

1. Wang, Z.; Qian, J.; Cao, L.; Wang, S.; Wen, T. A study of multilayer tape casting method for anode-supported planar type solid oxide fuel cells (SOFCs). *J. Alloys Compd.* **2007**, *437*, 264–268. [[CrossRef](#)]
2. Haile, S.M. Fuel cell materials and components. *Acta Mater.* **2003**, *51*, 5981–6000. [[CrossRef](#)]
3. Jung, G.B.; Lo, K.F.; Chan, S.H. Effect of pretreatments on the anode structure of solid oxide fuel cells. *J. Solid State Electrochem.* **2007**, *11*, 1435–1440. [[CrossRef](#)]
4. Minh, N.Q. Ceramic fuel cells. *J. Am. Ceram. Soc.* **1993**, *76*, 563–588. [[CrossRef](#)]
5. Chen, C.C.; Nasrallah, M.M.; Anderson, H.U. Synthesis and characterization of YSZ thin film electrolytes. *Solid State Ion.* **1994**, *70*, 101–108. [[CrossRef](#)]
6. Souza, S.D.; Visco, S.J.; Jonghe, L.C.D. Thin-film solid oxide fuel cell with high performance at low-temperature. *Solid State Ion.* **1997**, *98*, 57–61. [[CrossRef](#)]
7. Kim, J.W.; Virkar, A.V.; Fung, K.Z.; Mehta, K.; Singhal, S.C. Polarization effects in intermediate temperature, anode-supported solid oxide fuel cells. *J. Electrochem. Soc.* **1999**, *146*, 69–78. [[CrossRef](#)]
8. Lee, H.Y.; Oh, S.M. Origin of cathodic degradation and new phase formation at the La_{0.9}SrO_{0.1}MnO₃/YSZ interface. *Solid State Ion.* **1996**, *90*, 133–140. [[CrossRef](#)]
9. Liu, Y.; Hashimoto, S.; Nishino, H.; Takei, K.; Mori, M. Fabrication and characterization of a co-fired La_{0.6}Sr_{0.4}Co_{0.2}Fe_{0.8}O_{3-δ} cathode-supported Ce_{0.9}Gd_{0.1}O_{1.95} thin-film for IT-SOFCs. *J. Power Sources* **2007**, *164*, 56–64. [[CrossRef](#)]
10. Bao, W.; Chang, Q.; Meng, G. Effect of NiO/YSZ compositions on the co-sintering process of anode-supported fuel cell. *J. Membr. Sci.* **2005**, *259*, 103–109. [[CrossRef](#)]
11. Besra, L.; Zha, S.; Liu, M. Preparation of NiO-YSZ/YSZ bi-layers for solid oxide fuel cells by electrophoretic deposition. *J. Power Sources* **2006**, *160*, 207–214. [[CrossRef](#)]
12. Leng, Y.J.; Chan, S.H.; Khor, K.A.; Jiang, S.P. Performance evaluation of anode-supported solid oxide fuel cells with thin film YSZ electrolyte. *Int. J. Hydrog. Energy* **2004**, *29*, 1025–1033. [[CrossRef](#)]

13. Fabbri, E.; Pergolesi, D.; Traversa, E. Materials challenges toward proton-conducting oxide fuel cells: A critical review. *Chem. Soc. Rev.* **2010**, *39*, 4355–4369. [[CrossRef](#)] [[PubMed](#)]
14. Wachsmann, E.D.; Lee, K.T. Lowering the temperature of solid oxide fuel cells. *Science* **2011**, *334*, 935–939. [[CrossRef](#)] [[PubMed](#)]
15. Chroneos, A.; Yildiz, B.; Tarancon, A.; Parfitt, D.; Kilner, J.A. Oxygen diffusion in solid oxide fuel cell cathode and electrolyte materials: Mechanistic insights from atomistic simulations. *Energy Environ. Sci.* **2011**, *4*, 2774–2789. [[CrossRef](#)]
16. De Jonghe, L.C.; Jacobson, C.P.; Visco, S.J. Supported electrolyte thin film synthesis of solid oxide fuel cells. *Annu. Rev. Mater. Res.* **2003**, *33*, 169–182. [[CrossRef](#)]
17. Rupasov, D.; Chroneos, A.; Parfitt, D.; Kilner, J.A.; Grimes, R.W.; Istomin, S.Y.; Antipov, E.V. Oxygen diffusion in $\text{Sr}_{0.75}\text{Y}_{0.25}\text{CoO}_{2.625}$: A molecular dynamics study. *Phys. Rev. B* **2009**, *79*, 1–4. [[CrossRef](#)]
18. Seymour, I.D.; Tarancón, A.; Chroneos, A.; Parfitt, D.; Kilner, J.A.; Grimes, R.W. Anisotropic oxygen diffusion in $\text{PrBaCo}_2\text{O}_{5.5}$ double perovskites. *Solid State Ion.* **2012**, *216*, 41–43. [[CrossRef](#)]
19. Timakul, P.; Jinawath, S.; Aungkavattana, P. Fabrication of electrolyte materials for solid oxide fuel cells by tape-casting. *Ceram. Int.* **2008**, *34*, 867–871. [[CrossRef](#)]
20. Mücke, R.; Menzler, N.H.; Buchkremer, H.P.; Stover, D. Co-firing of thin zirconia films during SOFC manufacturing. *J. Am. Ceram. Soc.* **2009**, *92*, S95–S102. [[CrossRef](#)]
21. Moon, H.; Kim, S.D.; Park, E.W.; Hyun, S.H.; Kim, H.S. Characteristics of SOFC single cells with anode active layer via tape casting and co-firing. *Int. J. Hydrog. Energy* **2008**, *33*, 2826–2833. [[CrossRef](#)]
22. Park, H.G.; Moon, H.; Park, S.C.; Lee, J.J.; Yoon, D.; Hyun, S.H.; Kim, D.H. Performance improvement of anode-supported electrolytes for planar solid oxide fuel cells via a tape-casting/lamination/co-firing technique. *J. Power Sources* **2010**, *195*, 2463–2469. [[CrossRef](#)]
23. Moon, H.; Kang, D.W.; Park, H.G.; Hyun, S.H. Stress and camber analysis of anode-supported electrolytes by tape-casting and co-firing techniques. *Int. J. Hydrog. Energy* **2011**, *36*, 10991–10997. [[CrossRef](#)]
24. Malzbender, J.; Steinbrech, R.W.; Singheiser, L. A review of advanced techniques for characterizing SOFC behavior. *Fuel Cells* **2009**, *9*, 785–793. [[CrossRef](#)]
25. Shen, Z.; Zhu, X.; Le, S.; Sun, W.; Sun, K. Co-sintering anode and Y_2O_3 stabilized ZrO_2 thin electrolyte film for solid oxide fuel cell fabricated by co-tape casting. *Int. J. Hydrog. Energy* **2012**, *37*, 10337–10345. [[CrossRef](#)]
26. Menzler, N.H.; Malzbender, J.; Schoderbock, P.; Kauert, R.; Buchkremer, H.P. Sequential tape casting of anode-supported solid oxide fuel cells. *Fuel Cells* **2014**, *14*, 96–106. [[CrossRef](#)]
27. Cologna, M.; Contino, A.R.; Montinaro, D.; Sglavo, V.M. Effect of Al and Ce doping on the deformation upon sintering in sequential tape cast layers for solid oxide fuel cells. *J. Power Sources* **2009**, *193*, 80–85. [[CrossRef](#)]
28. He, C.R.; Wang, W.G.; Wang, J.; Xue, Y. Effect of alumina on the curvature, Young's modulus, thermal expansion coefficient and residual stress of planar solid oxide fuel cells. *J. Power Sources* **2011**, *196*, 7639–7644. [[CrossRef](#)]
29. Sun, B.; Rudkin, R.A.; Atkinson, A. Effect of thermal cycling on residual stress and curvature of anode-supported SOFCs. *Fuel Cells* **2009**, *9*, 805–813. [[CrossRef](#)]
30. Lia, W.; Hasinska, K.; Seabaugh, M.; Swartz, S.; Lannutti, J. Curvature in solid oxide fuel cells. *J. Power Sources* **2004**, *138*, 145–155. [[CrossRef](#)]
31. Jung, G.B.; Fang, L.H.; Chiou, M.J.; Nguyen, X.-V.; Su, A.; Lee, W.-T.; Chang, S.W.; Kao, I.C.; Yu, J.W. Effects of pretreatment methods on electrodes and SOFC performance. *Energies* **2014**, *7*, 3922–3933. [[CrossRef](#)]
32. Jung, G.B.; Fang, L.H.; Lin, C.Y.; Nguyen, X.-V.; Yeh, C.C.; Lee, C.Y.; Yu, J.W.; Chan, S.H.; Lee, W.-T.; Chang, S.W.; et al. Electrochemical performance and long-term durability of a reversible solid oxide fuel cell. *Int. J. Electrochem. Sci.* **2015**, *10*, 9089–9104.

